High-resolution digital holography utilized by the subpixel sampling method

Daniel Claus,[1,*] Marco Fritzsche,[2] Daciana Iliescu,[3] Brenda Timmerman,[3] and Peter Bryanston-Cross[3]

[1]Kroto Research Institute, University of Sheffield, S3 7HQ Sheffield, UK

[2]Visiting Student, Mechanical Engineering Department, Technische Universität Ilmenau, 98693, Germany

[3]School of Engineering, University of Warwick, CV4 7AL, Coventry, UK

*Corresponding author: d.claus@sheffield.ac.uk

Received 11 February 2011; revised 29 June 2011; accepted 30 June 2011; posted 5 July 2011 (Doc. ID 142484); published 10 August 2011

A novel (to our knowledge) approach for resolution improvement in digital holography is presented in this paper. The proposed method is based on recording the incoming interference field on a complementary metal-oxide semiconductor (CMOS) camera with subpixel resolution. The method takes advantage of the small pixel size of the CMOS sensor, while overcoming the reduced fill factor. This paper describes the experimental and numerical procedures. The improvement of the obtainable optical resolution, image quality, and phase measurement accuracy are demonstrated within this paper.

OCIS codes: 090.1995, 090.2880, 100.2980, 110.0180, 110.1650, 110.6150.

1. Introduction

In optical holography, the interference pattern, which results from the superposition of reference and object wave, is stored on a photographic plate. For most applications, photographic plates have been replaced by digital storage using charged coupled device (CCD) or complementary metal-oxide semiconductor (CMOS) sensors. The advantages of recording holograms in a digital format are faster image acquisition and simplified image processing. However, the typical resolution of CCD and CMOS sensors (200 lp/mm) is small compared to the typical resolution of holographic plates (3000 lp/mm). This restricts the maximum interference angle between reference and object wave. Consequently, a rather large distance between object and camera needs to be kept for the recording in order not to undersample the interference pattern. Because of the long recording distance, the optical resolution of the numerically reconstructed hologram is smaller than the resolution obtained with optical holography. The optical resolution can be calculated using Abbe's criterion, which is represented in Eq. (1). Moreover, inherent in a long recording distance is the appearance of larger speckles; see Eq. (2) adapted from [1], which results in a reduced image quality of the reconstructed hologram. To simplify the equations without loss of generality only the x component is considered here and hereafter.

$$\delta_x = \frac{\lambda d}{N_x \Delta x'}, \tag{1}$$

$$D''_{x\_\mathrm{speckle}} = \frac{2.44 \lambda d}{N_x \Delta x'}, \tag{2}$$

where D''_{x_speckle} is the speckle size in the x'' direction in the reconstruction plane (see Fig. 1 for nomenclature of planes), λ is the wavelength, N is the pixel number, $\Delta x'$ is the pixel size in the hologram plane, and d is the recording distance, which is a function of the pixel size. Taking into account the Nyquist

0003-6935/11/244711-09$15.00/0

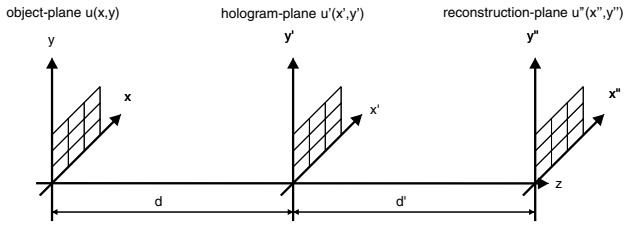

Fig. 1. Nomenclature for coordinates in object plane, hologram plane, and reconstruction plane.

criterion, the smallest recording distance for a Fresnel hologram [2] is

$$d_{\min} = \frac{(2x + N\Delta x')\Delta x'}{\lambda} \qquad \begin{cases} \text{in-line:} & x = X/2 \\ \text{off-axis:} & x = 1.5 \cdot X, \end{cases} \tag{3}$$

and for a Fourier hologram [3] is

$$d_{\min} = \frac{2x\Delta x'}{\lambda} \qquad \begin{cases} \text{in-line:} & x = X/2 \\ \text{off-axis:} & x = 1.5 \cdot X, \end{cases} \tag{4}$$

where X is the size of the object.

A commonly applied resolution improvement technique in digital holography is based on the synthetic aperture method, as presented in [4–7]. This method is based on either shifting a single sensor laterally by an amount equal to or slightly smaller than the sensor size (see [4,5,7]) or using laterally distributed multiple sensors (see [6]). Another way to implement the synthetic aperture method is based on tilted object illumination, in which the object is illuminated at different angles as discussed in [8]. All these implementations of the synthetic aperture method result in an increased numerical aperture, which results, as shown in Eq. (1), in an increased optical resolution.

Another way to improve the resolution is to sample the incident wave field with subpixel resolution, by which the effective sampling pixel size can be reduced. This allows the reduction of the recording distance, which results in an improvement of the optical resolution. Three different subpixel sampling resolution improvement methods have been reported in [9]. The three methods are based on laterally shifting the sensor by an amount smaller than the pixel size. The methods described by [9] were carried out with a CCD sensor of almost 100% fill factor. The subpixel sampling method described in this paper is based on CMOS technology. CMOS sensors have a smaller fill factor than CCD sensors. This results in a more reliable integrated irradiance when sampling the incoming wave field with subpixel resolution. Moreover, CMOS technology is cheaper than CCD technology, and it is available at smaller pixel sizes, which allow for a further resolution improvement. To the authors' knowledge, the smallest available pixel sizes for CMOS and CCD sensors are 1.4 μm (MT9E013, Aptina, USA) and 3.5 μm (ICX625, Sony, Japan), respectively. By comparison with CCD, one major drawback of CMOS sensors is their more noisy readout. The noisy readout can be reduced by hot-pixel elimination and dark-field calibration prior to the measurement. The dark-field data correspond to data recorded while no light enters the camera. The term hot pixel corresponds to a pixel that is continuously saturated independent of the magnitude of exposure applied. A minimization of both effects can be accomplished by recording an image with the laser switched off and the camera set at its experimental exposure parameters. The recorded image, which accommodates the dark field and hot pixels, needs to be subtracted from the recorded hologram.

2. Setup and Methodology

The experiment was performed using the setup schematically shown in Fig. 2. A He–Ne laser with a wavelength of 632.8 nm was used in the experiments. Before recording the hologram, the object was positioned at the minimum distance for the recording of Fresnel holograms, shown in Eq. (3). In order to obtain a good fringe contrast, the optical path length and polarization state [10] of reference and object wave have been matched. The hologram was then recorded on a 6.6 megapixel CMOS camera (C-Cam, BCi4-6600) with 3.5 μm pixel size and 35% fill factor. In order to increase the resolution of the numerically reconstructed hologram, the camera was moved closer to the object. At this distance, the recorded interference pattern is undersampled. The camera sensor was then moved with a backlash-free motorized PI M150.11 x–y stage with a linear resolution of 8.5 nm in the x' and y' directions by half the pixel size to four different positions, termed positions A, B, C, and D and shown in Fig. 3. After recording first in position A, the camera was horizontally shifted by half the pixel size to position B. From B, the camera was vertically shifted by half the pixel size to C. From C, the camera was horizontally shifted but in the opposite direction with respect to the A–B movement to arrive at D. Finally, from D the camera was vertically shifted back to its initial position. The holograms obtained at the four recording positions have then been combined into a hologram H. A simplified combination procedure for a 2 × 2 pixel array is shown in

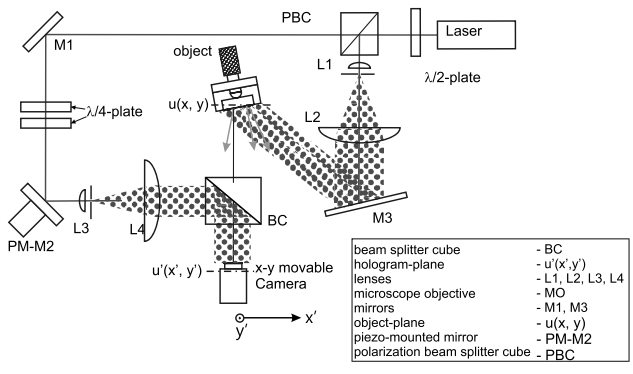

Fig. 2. Schematic diagram of experimental recording setup.

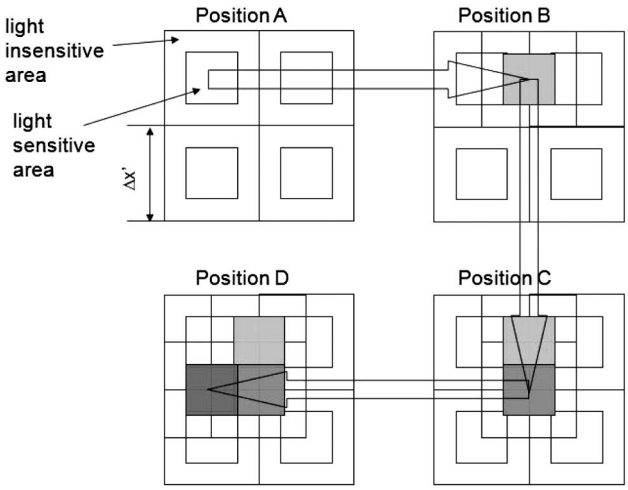

Fig. 3. Schematic diagram of the relative pixel positions for subpixel resolution sampling.

Fig. 4. In this manner, one original pixel was replaced by four subpixels of half the pixel size. The combination procedure can mathematically be described as follows:

$$\begin{aligned} H(2x'-1,2y'-1) &= A(x',y'),\\ H(2x'-1,2y') &= B(x',y'),\\ H(2x',2y') &= C(x',y'),\\ H(2x',2y'-1) &= D(x',y'). \end{aligned} \tag{5}$$

The recording mechanism on the digital target can be simulated by multiplying the continuously defined incoming wave-field intensity $u'(x')$ with a comb function, [see Eq. (6)]. The continuous values $u'(x')$ are transformed into discrete values $u'_d(x')$ separated by the pixel size (see Fig. 5),

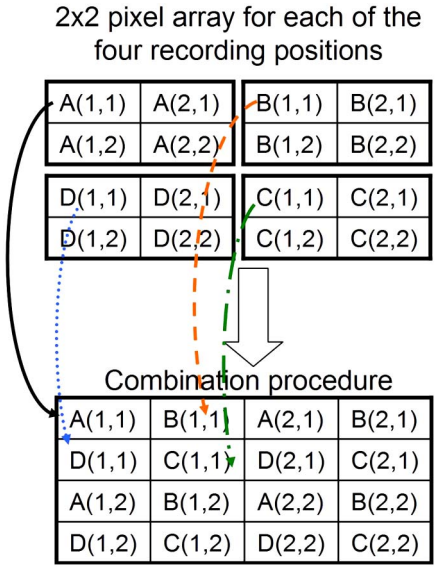

Fig. 4. (Color online) Combination procedure to obtain a subpixel hologram.

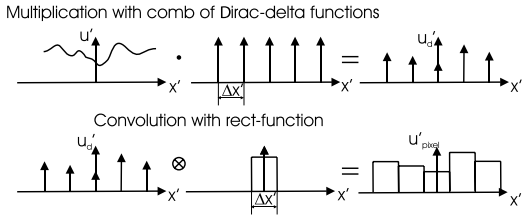

Fig. 5. Simulation of the digital recording mechanism.

$$u'_d(x') = u'(x')\mathrm{comb}\left(\frac{x'}{\Delta x'}\right). \tag{6}$$

The obtained result is convolved with a rect function of width $\Delta x'$ representing the impulse-response of the digital receiver (rectangular pixel area), which is represented in Eq. (7),

$$\begin{aligned} u'_{\mathrm{pixel}}(x') &= u'_d(x') \otimes \mathrm{rect}\left(\frac{x'}{\Delta x'}\right)\\ &= \mathcal{F}^{-1}[\mathcal{F}\{u'_d(x',y')\}\cdot \mathrm{sinc}(\nu_{x'}\Delta x')], \end{aligned} \tag{7}$$

where $\nu_{x'}$ is the spatial frequency in the x' direction in the hologram plane. The pixel modulation transfer function (MTF) is the absolute value of the transfer function, which is obtained by applying a Fourier transform to the rect function as discussed in [11],

$$\mathrm{MTF}_{\mathrm{pixel}} = |\mathrm{sinc}(\nu_{x'}\Delta x')|. \tag{8}$$

The pixel MTF contributes to the overall MTF of the optoelectrical system in a multiplicative manner. The benefits of using the subpixel sampling method in the recording process are

i. Reduced camera–object distance, by which a more detailed reconstruction is enabled and speckle-noise is reduced.
ii. Reduced camera–object distance, by which more object reflected and diffracted light is recorded. Hence electronic noise in the recording process is reduced.
iii. Higher cutoff frequency than when recording with the sensor-specified pixel size; see Fig. 6.
iv. Higher contrast recording of spatial frequencies ($0 < \nu_{x'} < \nu_{\text{sub-pixel}}$); see Fig. 6.
v. Fill factor maximized to 100%.

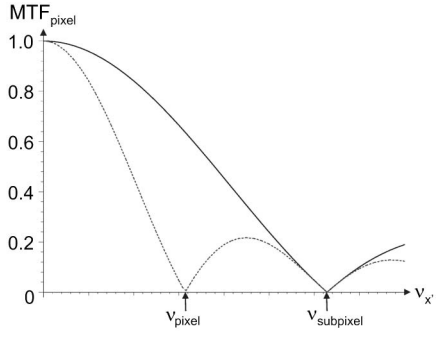

Fig. 6. Pixel MTF for the normal pixel size (dotted curve) and half the pixel size employing the subpixel sampling method (solid curve).

When performing the experiment, it was realized that, due to environmental perturbations, the interference fringes shifted randomly in the x' and y' directions. Phase stepping was introduced to minimize the influence of the environment on the measurement. The introduction of phase stepping results in an averaged fringe position. In addition, it enables the application of an in-line setup, which allows a further reduction of object–camera distance [Eqs. (3) and (4)] and consequently results in an increased optical resolution [Eq. (1)] and reduced speckle noise [Eq. (2)]. The analysis of the phase-stepped intensity holograms was based on a three-bucket phase-stepping algorithm developed by [12]. This algorithm calculates each individual phase step; hence it does not require environmental stability. At each of the four recording positions (see Fig. 3), three phase-stepped holograms were recorded. The phase step was implemented by a piezo-mounted mirror in the reference arm. After applying the phase-stepping algorithm, a phase map at each recording position is obtained. The four phase maps, one from each recording position, are then combined into a common phase map applying the combination procedure previously discussed [see Eq. (5)]. The initial phase among the four phase maps might differ. This would result in sudden phase jumps between adjacent pixels in the combined phase map as shown in Fig. 7(b). In this case, the combined phase map acts like a phase binary grating, which, when reconstructed, results in additional diffraction orders. These additional diffraction orders cause a splitting of the object information [see Fig. 7(b)], which results in a less detailed reconstruction. This problem can be overcome in two different ways. First, the different diffraction orders can be superimposed using cross correlation, and second, by phase adjustment of each individual phase map. The phase adjustment is performed by resizing a part (200×200 pixels) of the first phase hologram A to twice its size. The interpolated phase value of the resized hologram A' serves as a reference phase for the other three phase maps B, C, and D. For instance, in order to find the phase difference for B with respect to A, a new matrix B' is generated. The finding of B' can be considered to be the reversed process of the combination process represented in Eq. (5). Matrix B' can hence be calculated as

$$B'(x',y') = A'(2x'-1, 2y'). \tag{9}$$

The phase difference $\Delta\varphi_B$ is then calculated by averaging the difference between the initial matrix and the new matrix:

$$\Delta\varphi_B = \frac{1}{NM}\sum_{x'=1}^{N}\sum_{y'=1}^{M}(B(x',y') - B'(x',y')). \tag{10}$$

The resulting phase difference $\Delta\varphi_B$ is then subtracted from B in order to obtain the corrected phase difference map. In the same manner, the phase difference for C and D is determined and corrected. A schematic diagram of the phase-correction approach is shown in Fig. 8.

The final combined phase map possesses a smooth phase transition, which results in a reduced appearance of higher diffraction orders in the reconstruction process; see Fig. 7(c).

The reconstructed hologram was obtained using the Fresnel propagation method described mathematically in Eq. (11),

$$\begin{aligned} u(x'',y'') = \frac{i\exp(ikd')}{\lambda d'}\exp\left[\frac{i\pi}{\lambda d'}(x''^2 - y''^2)\right] \\ \cdot \mathcal{F}\left\{u(x',y')\mathrm{ref}^*(x',y') \right. \\ \left. \times \exp\left(\frac{i\pi}{\lambda d'}(x'^2 + y'^2)\right)\right\}, \end{aligned} \tag{11}$$

where ref^* is the complex conjugated reference wave.

For comparison of the subpixel sampling method with the normal recording process, holograms recorded from a cantilever as the object under investigation [see Fig. 9(a)] have been recorded at two camera–object distances, namely 191 mm and 300 mm. For the first distance, using the 3.5 μm pixel size consequently violates the Nyquist criterion. Aliasing occurs, which results in the appearance of ghost images in the reconstructed hologram; see Fig. 7(a), left side. These artifacts can be avoided using the subpixel sampling method, which is consequently employed at this distance. For the second distance, at the same pixel size the recorded hologram is not undersampled, therefore the standard process does not result in the appearance of ghost images. To illustrate the results obtained from both processes, a small region of interest of the object shown in Fig. 9(a) is selected for the intensity reconstructions shown in Figs. 9(b) and 9(c).

In order to evaluate the image quality of the reconstructions, the signal-to-noise ratio (SNR) was applied. The SNR can be calculated as

$$\mathrm{SNR} = 20\log\left(\frac{\bar{X}}{\sigma}\right), \tag{12}$$

where $\bar{X}$ is the mean value of a population and σ the standard deviation. Assuming that the noise is evenly distributed over the entire reconstructed hologram, only a small representative region of interest with ideally constant gray level needs to be considered for the calculation of the SNR. Gray level changes in that region should then solely be due to noise. The SNR values for the reconstructions are 25.18 dB when applying the subpixel sampling method as shown in Fig. 9(b) and 22.71 dB using the camera specified pixel size; reconstruction is shown in Fig. 9(c).

The subpixel sampling method has also been applied to double-exposure holography. The recording distance was again chosen to produce an undersampled hologram for the 3.5 μm pixel size. The cantilever was deflected in an axial direction (z) by

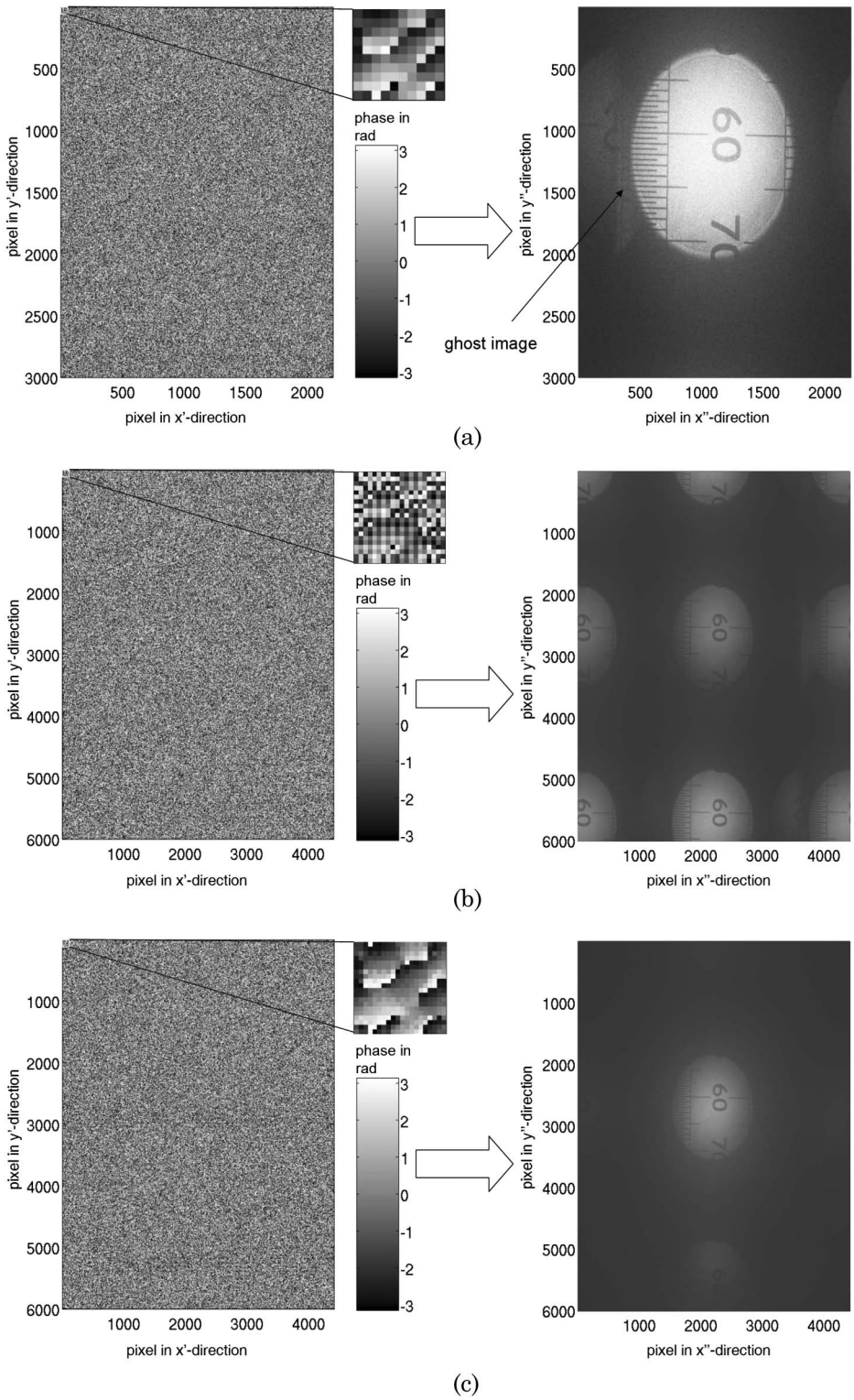

Fig. 7. Phase hologram and reconstruction at 191 mm recording distance for (a) an undersampled normal hologram with 3.5 μm pixel size, (b) subpixel sampled hologram without phase correction, and (c) subpixel sampled hologram with phase correction.

2 mm in order to produce a high density of fringes in the double-exposure phase map. Because of the high density of fringes, only small regions of the double-exposure phase maps are shown in Fig. 10. The 2π discontinuity map can be resolved to a greater degree when employing the subpixel sampling method in comparison to the reconstruction with 3.5 μm pixel size. This is also shown in the values for standard deviation, which for 3.5 μm is 1.76 rad and for 1.75 μm pixel size is 1.72 rad. The standard deviation, which represents the measurement uncertainty obtained with the system, is more meaningful for

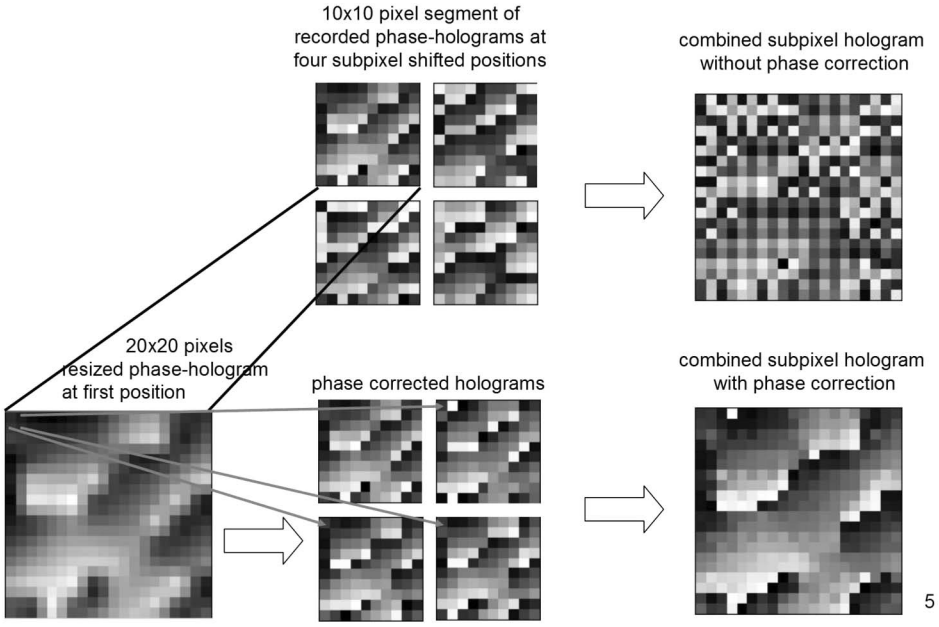

Fig. 8. Schematic diagram of the phase-correction procedure.

phase reconstruction than the previously used SNR for the intensity reconstruction. Taking into account the setup geometry, the corresponding deformation measurement uncertainties are $\frac{\lambda}{6.88}$ for 3.5 μm and $\frac{\lambda}{7.05}$ for 1.75 μm, respectively. Thus the double-exposure phase map obtained with the subpixel sampling method can resolve to a higher degree of accuracy.

3. USAF-1951 Test Target

In order to determine the resolution improvement when applying the subpixel sampling method, the USAF 1951 test target was used as the object of study. The setup used originally was changed to a transmission setup by replacing the object with a mirror. Moreover, the plane reference wave was replaced by a spherical wave, as shown in Fig. 11. This enabled the recording of Fourier holograms, by which the sensor's space–bandwidth product (SBP) is used more efficiently.

The transparent USAF-1951 test target was placed between mirror $M4$ and the beam splitter. An intensity hologram was then recorded without applying the subpixel method at a recording distance of 295 mm. Zero-padding, as discussed in [1], was applied to generate a hologram of equal dimensions in the x and y directions. In this manner, the reconstructed hologram does not suffer from different pixel sizes $\Delta x''$ and $\Delta y''$ in the reconstruction plane [Eq. (13)], which otherwise would result in a

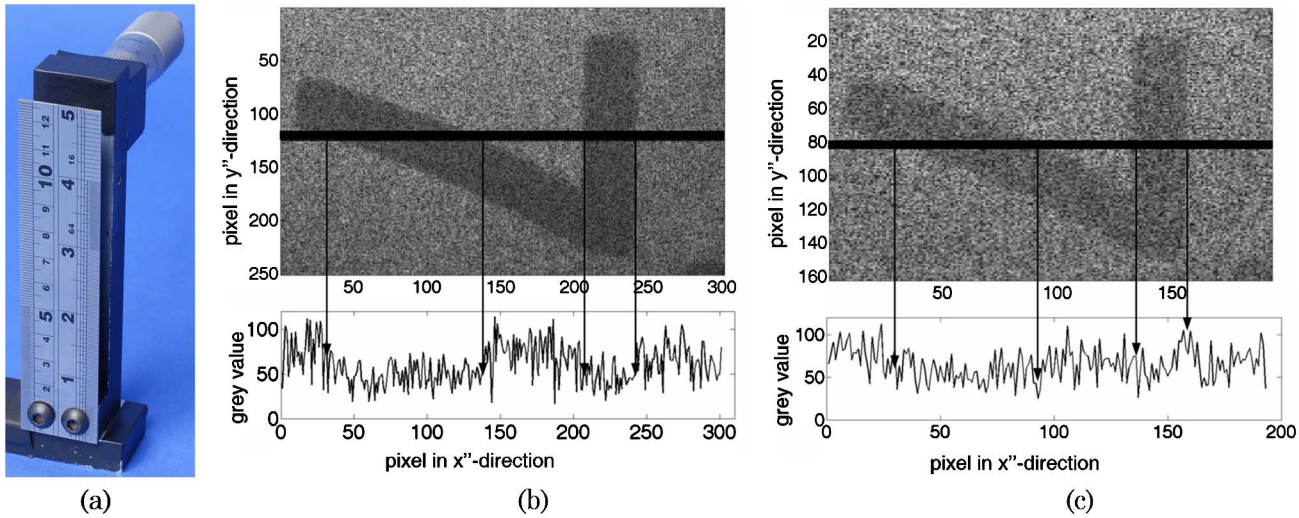

Fig. 9. (Color online) (a) Cantilever with micrometer screw used for experiments, region of interest for intensity reconstruction and their profile lines for (b) subpixel sampled hologram at 191 mm recording distance and (c) normal hologram with 3.5 μm pixel size at 300 mm recording distance.

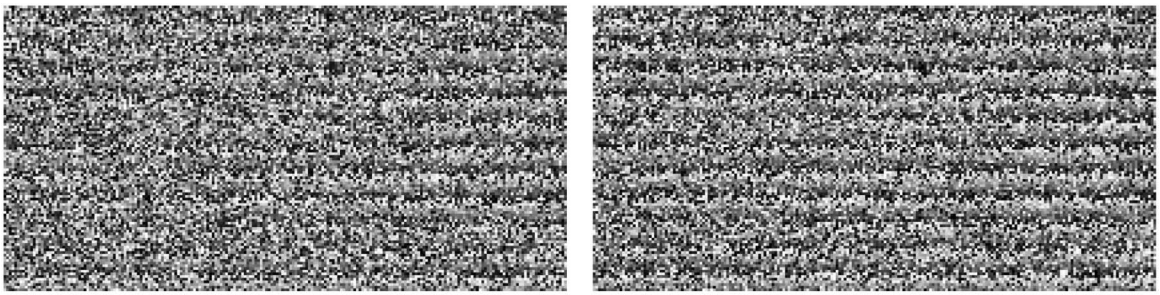

(a) (b)

Fig. 10. Segment of double-exposure phase maps for 191 mm recording distance (a) normal hologram with 3.5 μm pixel size, (b) subpixel sampled hologram with 1.75 μm pixel size.

distorted (stretched) reconstruction and might produce different horizontal and vertical resolution and depth of field:

$$\Delta x'' = \frac{\lambda d'}{N \Delta x'}. \tag{13}$$

Afterwards the recording distance was reduced to 185 mm, at which the subpixel sampling method was applied. The recorded intensity hologram at a 295 mm recording distance, the modulus of the complex object wave for the subpixel sampled hologram, and their corresponding numerical reconstructions are shown in Fig. 12. In order to observe the smallest resolvable test-target element, a small region has been selected, shown in Figs. 12(e) and 12(f). Rather than only taking a single cross section for a considered test-target element into account, the optical resolution was determined by averaging all cross sections across the test-target element under investigation. This enabled a more accurate determination of the optical resolution obtained. The averaged cross sections are shown in Figs. 12(e) and 12(f), where the x axis denotes the pixel number and the y axis the normalized intensity. Care was taken so that the three local minima (black strips) are visible and the ratio of the largest local minima to the smallest local maxima is less than 0.81 according to the resolution criterion. The black ring in Fig. 12 encircles the horizontal resolution and the white ring the vertical resolution.

In order to have a more complete evaluation of the optical system's information capacity, the SBP was calculated. The SBP represents the product of the field of view and the highest resolvable spatial frequency. The SBP is a more meaningful parameter for the judgment of optical systems, since it is independent from the recording distance and permits the comparison of different optical systems. The optimum SBP is obtained when recording an in-line Fourier hologram,

$$\mathrm{SBP}_{\text{in-line}} = N \cdot M, \tag{14}$$

where N and M are the pixel numbers for both lateral sensor dimensions. For an off-axis Fourier hologram, the $\mathrm{SBP}_{\text{off-axis}}$ is a quarter of the $\mathrm{SBP}_{\text{in-line}}$, as discussed in [13]. In order to measure the setup performance with respect to its optimum SBP, an efficiency parameter, η, is introduced:

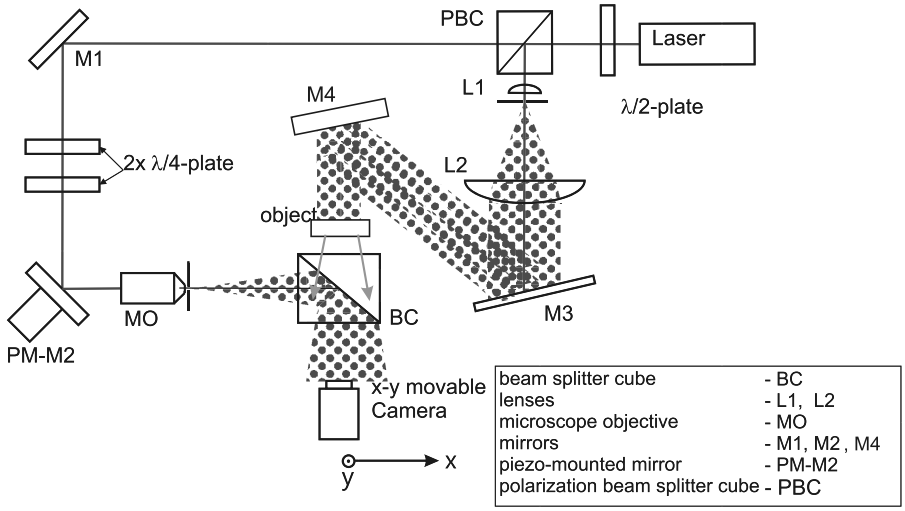

Fig. 11. Transmission setup for the recording of a Fourier hologram.

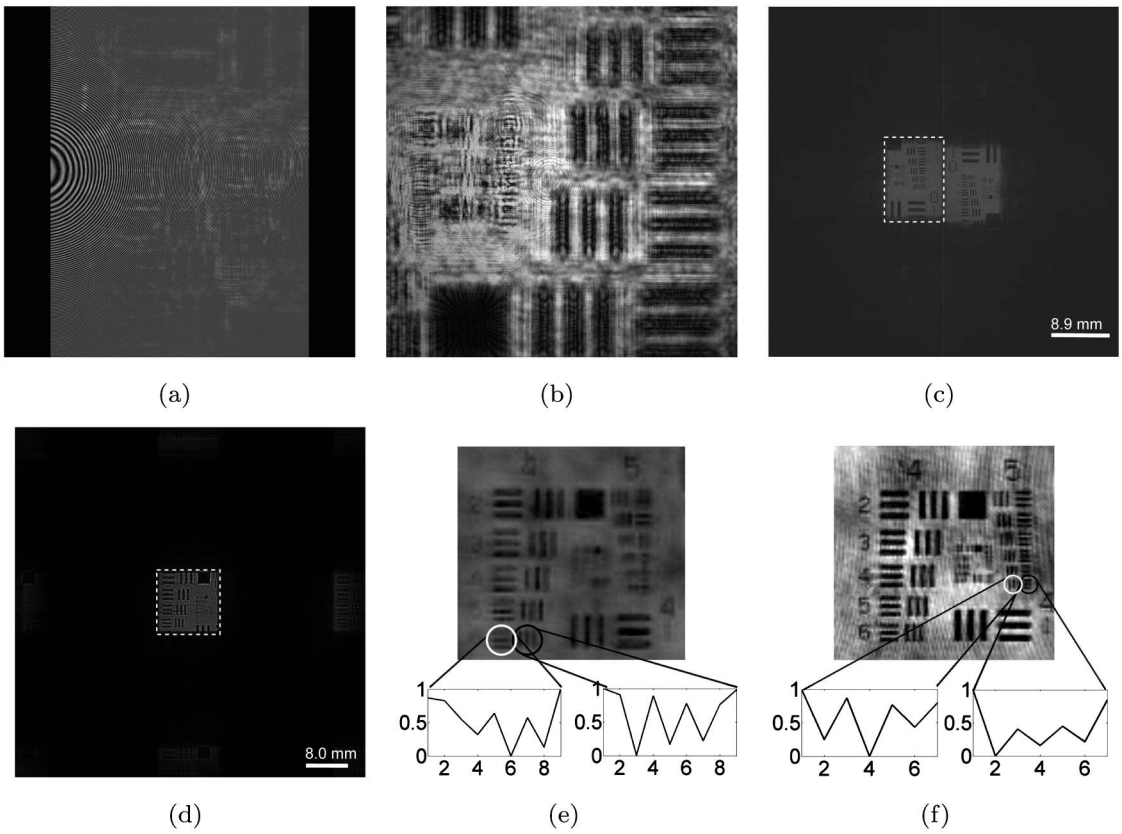

Fig. 12. (a) Recorded intensity hologram 3000 × 3000 pixels, (b) modulus of calculated complex object wave 6000 × 6000 pixels, numerical reconstructions with field of view indicated by dashed line (c) without subpixel sampling method, (d) with subpixel sampling method, and (e), (f) corresponding areas of interest to determine smallest resolvable element.

$$\eta = \frac{\mathrm{SBP}}{\mathrm{SBP}_{\text{in-line}}}. \tag{15}$$

In this manner, different optical setups can be compared. The theoretically possible resolution according to Eq. (1), the achieved resolution, the SBP, and η for both hologram are shown in Figs. 12(a) and 12(b), and the results from two recent papers [7,14] are shown in Table 1. The field of view was obtained by multiplication of the pixel size in the reconstruction plane with the number of pixels displaying the reconstructed image [highlighted by a dashed white line in Figs. 12(c) and 12(d)]. The results obtained could be confirmed by comparison with the real physical USAF test target.

In conclusion, it was found that the result obtained for the maximum resolution matches well with the expected value. Furthermore, the SBP and the η obtained can compete with the results published in recent papers [7,14]. A larger field of view was expected, which would have led to a larger SBP and η. Only a small part of the reconstructed hologram displays the image, shown in Fig. 12(d). The reduced field of view is due to the use of a transparent object. Diffraction only occurs at the edges of the target bar elements. The major part of the recorded light is undiffracted. A collimated laser beam was used to illuminate the USAF test target. Thus the size of the undiffracted recorded light corresponds to the projection of the sensor onto the object. In that manner, diffracted light that originates from object points outside the projected sensor area is recorded with almost no background intensity. This results in a reduction of visibility for the corresponding object

Table 1. Theoretical and Practically Achieved Resolution

Reconstruction	3000 × 3000 at 295 mm	6000 × 6000 at 185 mm	5000 × 5000 from Ref. [14]	8000 × 8000 from Ref. [7]
Maximum theoretical resolution (μm)	17.8 @ 632 nm	11.2 @ 632 nm	—	6.7 @ 632 nm
Achieved vertical resolution (μm)	17.5	8.7	2.6	6.2
Achieved horizontal resolution (μm)	17.5	8.7	2.6	7.8
Field of view (mm^2)	9.0 × 12.1	11.7 × 11.7	4 × 4	30 × 23
SBP (10^6)	0.36	1.79	2.37	14.27
η (%)	3.96	4.95	9.5	22.3

region. Using a diffuse reflective test target would result in a homogeneous object information distribution across the recorded hologram, and should therefore yield a larger field of view for the reconstructed hologram.

4. Conclusion and Discussion

A novel (to our knowledge) approach to improve the optical resolution of digital holograms based on subpixel sampling of the incident interference pattern in conjunction with the application of CMOS technology and phase stepping was presented in this paper. The low fill factor inherent in CMOS technology could be maximized to 100%. The successful implementation of the subpixel method was shown for an intensity-reconstructed hologram and double-exposure hologram of a cantilever. The image quality improvement for these reconstructions was demonstrated by calculating the SNR. Holograms with normal pixel size and with the subpixel sampling method were recorded and reconstructed to prove the resolution improvement. A resolution improvement and an increase of the SBP could be demonstrated.

The system as it stands at the moment is limited to static measurements due to shifting the camera to four positions at each of which phase stepping is applied. Potentially, real time measurement can be carried out by minimizing the environmental perturbations. This would result in a good laterally localized incoming wave field with respect to the pixel size employed. Rather than recording 12 holograms, only four holograms, one for each shifting position, need to be recorded, which would significantly speed up the acquisition time. The reduction of environmental perturbations can be accomplished by the application of, for example, common path interferometry or shearing interferometry. The shift to the four recording positions and the camera frame rate need to be aligned. Moreover, both camera frame rate and shift speed need to be large enough to avoid speckle decorrelation caused by the object movement. Speckle decorrelation needs to be less than half the speckle size, according to [1], while recording the four laterally subpixel-shifted holograms. Thus the frame rate and translation stage shifting velocity required is determined by the frequency of the dynamic event.

In case the environmental perturbations are still very strong, the subpixel sampling method as described in the main body of the paper may need to be applied. The investigation of dynamic events would be limited; however, they would still be feasible for dynamic events of small temporal frequency.

Another possible application of the subpixel sampling method is for digital holographic microscopy. The usage of a high NA system of relatively small magnification would be enabled, such as a Nikon CFI Apo LWD 25XW (25×, NA = 1.1), Nikon Corp., Japan. The application of such a microscope objective would result in an increased FOV and hence an increased SBP.

The applications and improvements discussed above could be the basis of future work for this method.

This project was supported by the Innovative Manufacturing Research Centre, project R.ESCM 9231. We would like to express our gratitude to Prof. Derek Chetwynd, who generously allowed us to use some of his equipment. Last, but not least, we would like to thank the School of Engineering technicians for manufacturing the devices needed in the scope of these experiments.

References and Notes

1. T. Kreis, *Handbook of Holographic Interferometry: Optical and Digital Methods* (Wiley-VCH, 2005).
2. Interference of object wave with a plane reference wave.
3. Interference of object wave with a spherical reference wave that originates from the object plane.
4. F. Le Clerc and M. Gross, "Synthetic-aperture experiment in the visible with on-axis digital heterodyne holography," Opt. Lett. **26**, 1550–1552 (2001).
5. J. H. Massig, "Digital off-axis holography with a synthetic aperture," Opt. Lett. **27**, 2179–2181 (2002).
6. T. Kreis and K. Schlüter, "Resolution enhancement by aperture synthesis in digital holography," Opt. Eng. **46**, 055803 (2007).
7. D. Claus, "High-resolution digital holographic synthetic aperture applied to deformation measurement and extended depth of field method," Appl. Opt. **49**, 3187–3198 (2010).
8. L. Granero, V. Micó, Z. Zalevsky, and J. Garcia, "Synthetic aperture super-resolved microscopy in digital lensless Fourier holography by time and angular multiplexing of the object information," Appl. Opt. **49**, 845–857 (2010).
9. J. Kornis and B. Gombköto, "Application of super image methods in digital holography," Proc. SPIE **5856**, 245–253 (2005).
10. Obtained by rotation of two quarter-wave plates in the reference arm.
11. G. D. Boreman, *Modulation Transfer Function in Optical and Electro-Optical Systems* (SPIE Press, 2001), Vol. TT52.
12. L. Z. Cai, Q. Liu, and X. L. Yang, "Generalized phase-shifting interferometry with arbitrary unknown phase steps for diffraction objects," Opt. Lett. **29**, 183–185 (2004).
13. A. W. Lohmann and S. Sinzinger, *Optical Information Processing* (Universitätsverlag Ilmenau, 2006).
14. J. Di, J. Zhao, H. Jiang, P. Zhang, Q. Fan, and W. Sun, "High-resolution digital holographic microscopy with a wide field of view based on a synthetic aperture technique and use of linear CCD scanning," Appl. Opt. **47**, 5654–5659 (2008).